ASTROBIOLOGY
Volume 18, Number 8, 2018
© Mary Ann Liebert, Inc.
DOI: 10.1089/ast.2017.1799

Speciation of Paleoarchean Life Demonstrated by Analysis of the Morphological Variation of Lenticular Microfossils from the Pilbara Craton, Australia

Kenichiro Sugitani,[1] Takashi Kohama,[1] Koichi Mimura,[1] Makoto Takeuchi,[1] Ryoko Senda,[2,*] and Hiroshi Morimoto[1]

Downloaded by 185.50.251.62 from www.liebertpub.com at 08/28/18. For personal use only.

Abstract

The ca 3.4 Ga Strelley Pool Formation (SPF) of the Pilbara Craton, Australia, represents a Paleoarchean sedimentary succession preserving well-described and morphologically diverse biosignatures such as stromatolites and cellularly preserved microfossils. The SPF microfossil assemblage identified from three greenstone belts includes relatively large (20–80 μm in width), acid-resistant, organic-walled lenticular microfossils, which can be extracted using a palynological technique. In this study, we present results of measurements of over 800 palynomorphic specimens of SPF lenticular microfossils from 2 remote (~80 km apart) localities that represent different depositional environments and thus different habitats, as evidenced by their distinct lithostratigraphic association and trace element geochemistry. We demonstrate statistically that the two populations are distinct in oblateness from a polar view and furthermore that each population comprises subpopulations defined by different areas and oblateness. This study may provide the earliest morphological evidence for speciation of unicellular organisms, which could have been allopatric (geographic) and adaptive. It can also be suggested that SPF lenticular microbes had highly organized cytoskeleton indispensable for strict control of the cell morphology of large and robust microbes, which in turn were likely advantageous to their prosperity and diversification. Key Words: Strelley Pool Formation—Lenticular microfossils—Paleoarchean—Speciation. Astrobiology 18, 1057–1070.

1. Introduction

Since the 1960s, numerous efforts to discover traces of early life have been made (*e.g.*, Barghoorn and Tyler, 1965; Cloud, 1965; Engel *et al.*, 1968), and through debates on biogenicity of some described putative microfossils (*e.g.*, Schopf, 1976; Schopf and Walter, 1983; Buick, 1984; Awramik *et al.*, 1988; Brasier *et al.*, 2002; Schopf *et al.*, 2002), it has now become accepted that microbes had already composed complex ecosystems on the Paleoarchean Earth (*e.g.*, Walsh and Lowe, 1985; Allwood *et al.*, 2006; Van Kranendonk, 2007; Javaux *et al.*, 2010; Sugitani *et al.*, 2010, 2013, 2015a; Wacey *et al.*, 2011; Homann *et al.*, 2016; Kremer and Kaźmierczak, 2017; Oehler *et al.*, 2017; Schopf *et al.*, 2017, 2018). The microfossils that have been documented are morphologically diverse, including distinct types such as thin threads, hollow and thick tubes, segmented tubes, small spheroids, large spheroids, and lenses. Because of the age of the rocks, genetic information is unavailable, but this morphological diversity implies that microbial speciation occurred during the Paleoarchean. Detailed work on Paleoarchean filamentous putative microfossils (Schopf, 1993) may provide morphological evidence for speciation. Until now, however, there have not been any systematically performed statistic studies focused on speciation of Paleoarchean microbes, in part, because of the difficulties in quantifying their morphological variations in petrographic thin sections. In this study, we describe speciation of Paleoarchean life based on detailed morphological characterization of lenticular microfossils from the ca. 3.4-Ga Strelley Pool Formation (SPF) of the Pilbara Craton, Australia. The results of measurements of over 800 palynomorphic specimens from 2 remote (>80 km apart) localities of the SPF are presented, statistically demonstrating species diversity of Paleoarchean life.

[1]Department of Earth and Environmental Sciences, Graduate School of Environmental Studies, Nagoya University, Nagoya, Japan.
[2]Japan Agency for Marine-Earth Science and Technology, Yokosuka, Japan.
*Present address: Graduate School of Integrated Sciences of Global Society, Kyushu University, Fukuoka, Japan.

Downloaded by 185.50.251.62 from www.liebertpub.com at 08/28/18. For personal use only.

2. Materials and Methods

2.1. Geological background and sample localities

The SPF has been identified widely in the East Pilbara Terrane; it is assumed that its depositional area was at least 30,000 km^2 (Hickman, 2008; Hickman and Van Kranendonk, 2008). The thickness of this formation is typically 8–11 m, although at some localities, it can be up to 100 m. Rocks of various types, including siliciclastic sedimentary rocks such as sandstone and shale, carbonates (mainly bedded and stromatolitic dolomite), chert, and volcaniclastic rock, compose this formation. The SPF represents various depositional environments, but mainly shallow water and even terrestrial settings, such as rocky coastal shoreline and beach; shallow water marine carbonate platform; possible sabkha; tidal flat; and alluvial fan, with or without hydrothermal inputs (Allwood *et al.*, 2006, 2007, 2010; Hickman, 2008; Sugitani *et al.*, 2015b).

Two localities ~80 km apart in the Goldsworthy and Panorama greenstone belts were selected for this study, from the known four SPF microfossil localities in the East Pilbara Terrane of the Pilbara Craton (Sugitani *et al.*, 2010, 2013) (Fig. 1), because of the prolific occurrence of microfossils. The SPF at the Goldsworthy locality comprised dominantly ~80-m-thick coarse- to very coarse-grained sandstone, with five interbedded cherty units 1.5–3 m in thickness. Fossil-bearing black chert occurs in the uppermost unit, which comprises sandstone containing flat cherty pebbles or angular chert clasts that suggest a high-energy environment and finely laminated black and black-white cherts that likely formed in a relatively low-energy environment (Fig. $2a_1$). This unit shows abrupt lateral facies change, and the fossil-bearing chert has conical structures that are interpreted as possible siliceous sinter formed in the terrestrial hydrothermal system (Fig. $2a_2$) (Sugitani *et al.*, 2015b). The SPF at the Panorama locality is a thin (~4 m in thickness) unit comprising a black to pale green to gray chert, a white chert breccia, and cross-laminated to thinly bedded pale to reddish-brown rock (Fig. $2b_1$). Microfossils are abundant in the microscopically fine laminated portion of the black chert (Fig. $2b_2$). A shallow (intertidal to subtidal) marine environment, with hydrothermal input, has been suggested as the environment of deposition for the Panorama SPF sediments (Allwood *et al.*, 2007, 2010; Sugitani *et al.*, 2013).

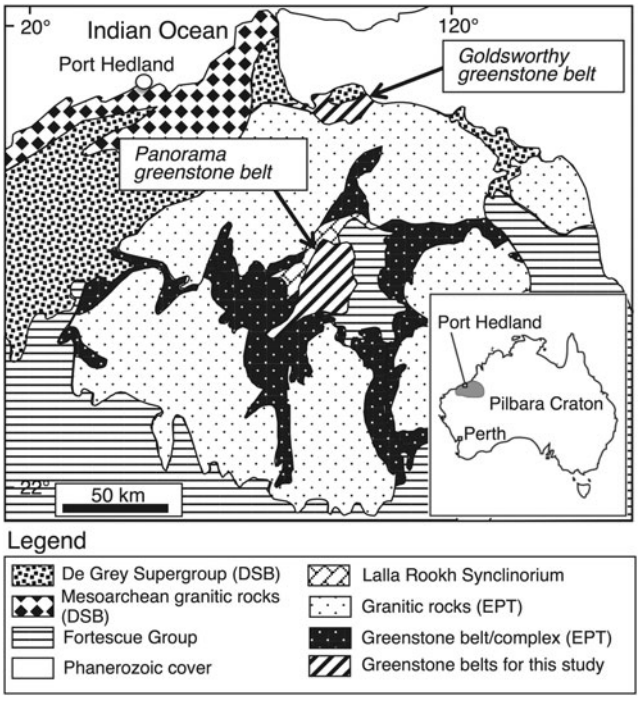

FIG. 1. Geology of Pilbara Craton and the locations of two greenstone belts from which lenticular microfossils of the SPF studied here were described. SPF, Strelley Pool Formation.

2.2. Palynology and microscopy

Extraction of lenticular microfossils through demineralization by acid (HF/HCl) maceration was performed at Nagoya University using a modification of a method described by Grey and Sugitani (2009). Pipetted specimens were mounted on glass slides with an aqueous mount medium (Mount-Quick ''Aqueous'' by COSMO BIO CO. LTD., Tokyo, Japan). Additionally, ca. 30-μm-thick polished sections of cherts were prepared. These slides were examined using a Leica DMRP microscope with 10×, 20×, 40×, and 100× magnification in plain, polarized transmitted light.

2.3. Major and trace element analyses

Ten subsamples from the fossil-rich black chert collected from the Panorama locality were subjected to major and trace element analyses, following a previously described method (Sugitani *et al.*, 2015b). For measurements of concentrations of rare earth element (+ yttrium) (REE+Y) and heavy metals (Cr, Co, Ni, Cu, Zn, As, and Pb), sample powders (500 mg to 3 g) were digested using HF and $HClO_4$ (HF: $HClO_4$ = 7:3). The sample solutions were dried on a hot plate (at 180°C) and then dissolved using 1.7 N-HCl, and supernatants were collected after centrifugation. Analyses were performed using an inductively coupled plasma mass spectrometer (ICP-MS; Agilent 7500ce) at the Japan Agency for Marine-Earth Science and Technology. Concentrations of some major elements (TiO_2, Al_2O_3, and Fe_2O_3) were determined by X-ray fluorescence (XRF) spectrometry (PANalytical Axios) at Nagoya University, using discs of fused glass made from a mixture of sample powder and $Li_2B_4O_7$ (1:5). Analytical results are listed in Table 2.

2.4. Size data measurements and statistical analyses

The SPF lenticular microfossils comprise a central body with a surrounding thin discoid flange of various widths. Mounting extracted specimens on glass slides enabled us to observe their equatorial views (Fig. 3a). Size data of lenticular microfossils in this direction (major and minor dimensions of both the whole and central bodies) (Fig. 3b) were measured using a digital camera DFC280 mounted on a Leica DMRP microscope and Leica Application Suite V.3.8.0. When more than three-fourths of the whole shape is preserved, the size was measured by extrapolation. There were 415 measured specimens for the Waterfall locality and 433 for the Panorama locality. The data were further examined using measured parameters (major and minor dimensions of the whole and

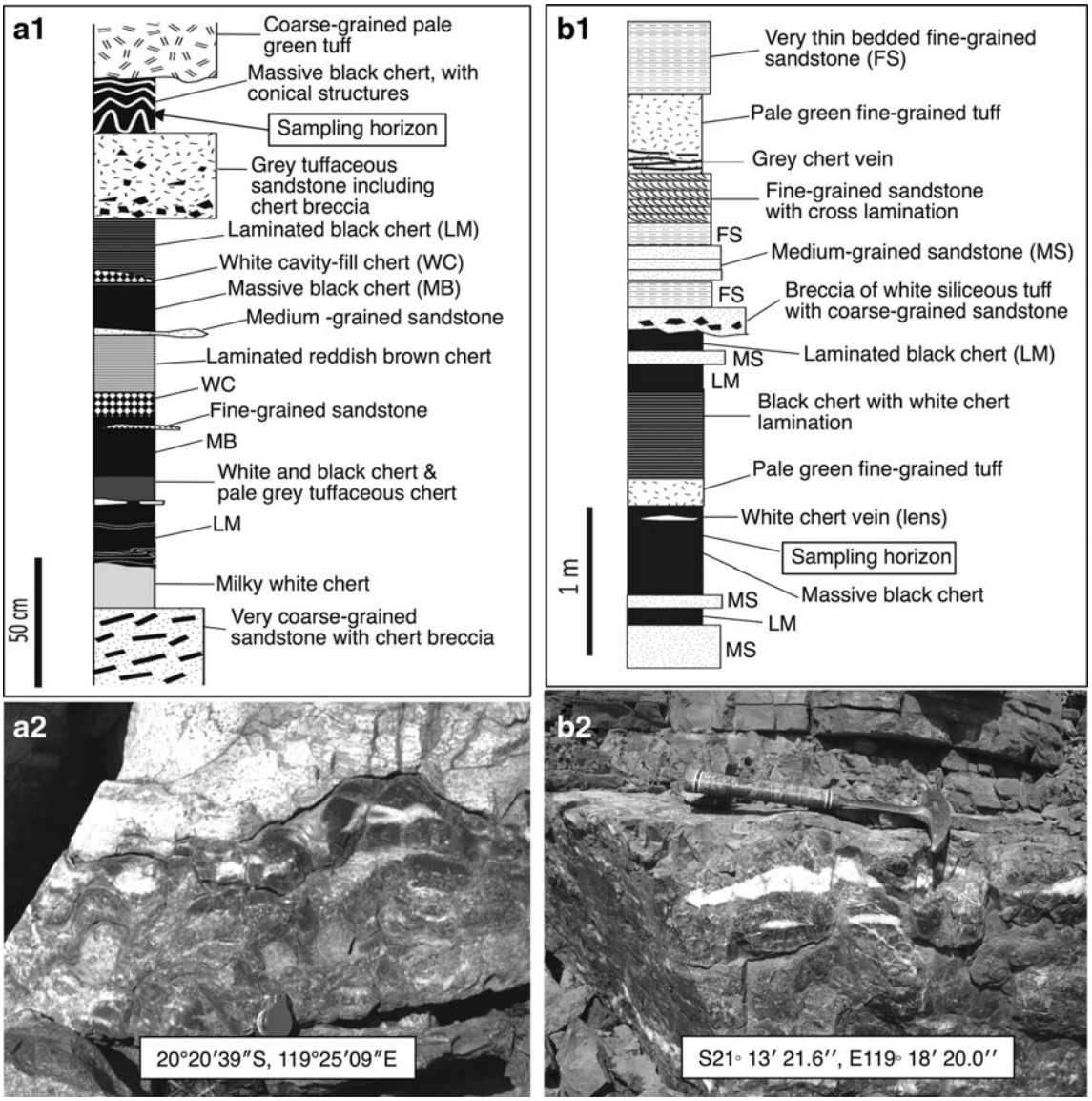

FIG. 2. **(a_1)** Lithostratigraphy of the SPF fossil site in the Goldsworthy greenstone belt. **(a_2)** Photograph of the outcrop of the Goldsworthy fossil-bearing black chert. A hand lens for scale. **(b_1)** Lithostratigraphy of the SPF fossil site in the Panorama greenstone belt. **(b_2)** Photograph of the outcrop of the Panorama fossil-bearing black chert. A hammer for scale.

Downloaded by 185.50.251.62 from www.liebertpub.com at 08/28/18. For personal use only.

central bodies), using the interquartile range method, and outliers were omitted. This resulted in final data of $n=395$ and $n=414$ for the Goldsworthy and Panorama populations, respectively. Oblateness was calculated as follows: (major dimension − minor dimension)/major dimension, whereas the flange ratio was calculated as follows: (area of the whole body − area of central body)/area of the whole body (Fig. 3). Cluster analyses were performed using Ward's method (after scaling of explanation variables) as Ward's method appeared to outperform the average linkage method. The results were described by hierarchical dendrograms.

3. Results and Discussion

3.1. Biogenicity of SPF lenticular microfossils

Biogenicity of SPF lenticular structures has been well demonstrated by a series of studies (Sugitani *et al.*, 2010, 2013, 2015a; Lepot *et al.*, 2013; Oehler *et al.*, 2017). In this study, we summarize the lines of evidence as follows.

(1) The lenticular structures are contained in primary cherts without any evidence of metasomatic replacement of precursory nonsiliceous sediments. The matrix, in which microfossils are embedded, is rich in cloudy carbonaceous particles (Fig. 4a), locally forming the lamination (Fig. 4b).
(2) Lenticular structures comprise carbonaceous matter with significantly light ($\delta^{13}C < -30$ per mil at Pee Dee Belemnite notation) isotopic values. Carbon isotopic values are heterogeneous even in a single specimen. The carbonaceous matter comprises an acid-resistant membrane and thus the structures can be extracted by HCl-HF maceration (Fig. 3a).
(3) Lenticular structures occur abundantly. The number of specimens identified in a petrographic thin section

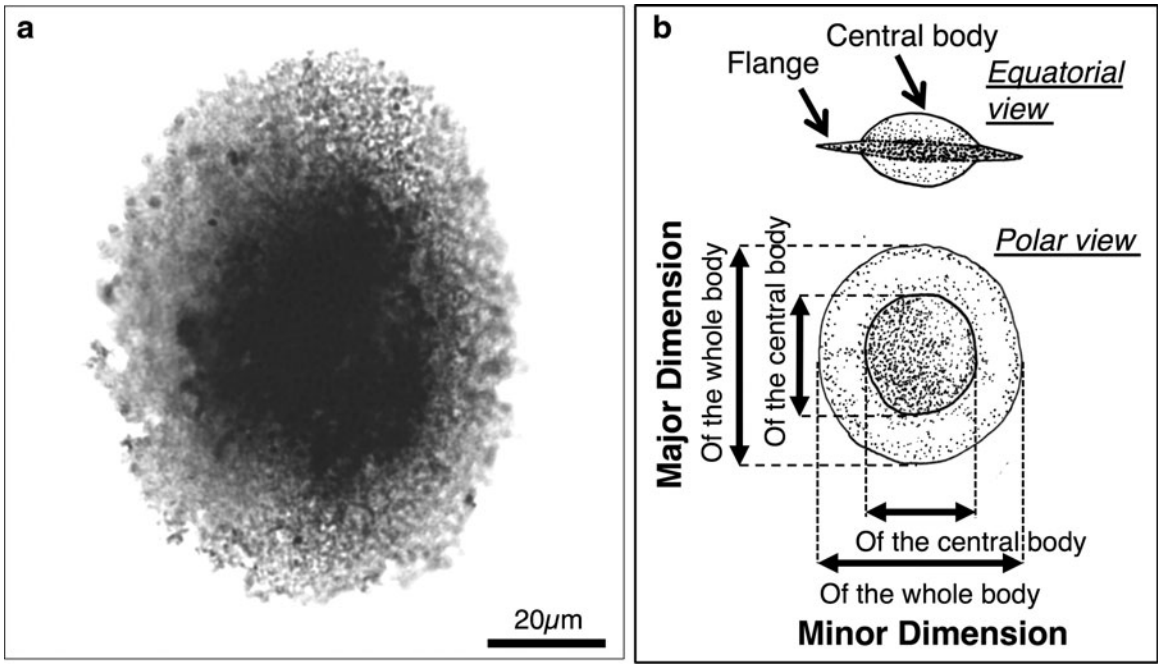

FIG. 3. **(a)** Polar view of a palynomorphic specimen of lenticular microfossil from the Panorama locality. **(b)** Schematic figures showing the basic body plan of lenticular microfossils.

Downloaded by 185.50.251.62 from www.liebertpub.com at 08/28/18. For personal use only.

(2.8×4.7 cm in width and 30 μm in thickness) can reach 100 or more. The structures often comprise colony-like clusters, including those comprising randomly oriented specimens, parallel-aligned specimens, and chained specimens (Fig. 4c–e). Paired specimens, corresponding to reproduction, are common (Fig. 5).

(4) Size distribution is within a range from 20 to 100 μm along the major dimension, although the population of lenticular microfossils comprises multiple morphologically defined subpopulations, as discussed in this study.

(5) Lenticular structures display various taphonomic features, such as deformation and breakage. Partial degradation of the flange or wall of the central body is common (Fig. 4f, g).

(6) Lenticular structures co-occur with other morphological types of carbonaceous structures that are best explained to be of biogenic origin, including spheroids, films, and rarely filaments.

(7) It should be emphasized that SPF microfossil assemblage and its equivalents have been identified from more than four localities in the three greenstone belts of the Pilbara Craton and also from the Kaapvaal Craton, South Africa (possibly Pflug, 1967; Walsh, 1992; Oehler *et al.*, 2017). They all occur in primary sedimentary cherts enriched in carbonaceous particles.

Lenticular microfossils are large and complex in morphology and have acid-resistant robust walls. These features suggest eukaryotic affinity, which does not fit the generally accepted scenario of the evolution of life (*e.g.*, Knoll, 2014). However, this cannot be taken as a reason for potentially dismissing their biogenicity. It is now widely known that some prokaryotes can be large and have complex morphology and even robust vesicles (Waterbury and Stanier, 1978; Schulz and Jørgensen, 2001; Salman *et al.*, 2013). In either case, we know little about the evolutionary contexts of Archean microfossils, and it is not reasonable to conclude that evolution and diversification have proceeded gradually and straightforwardly from a small simple cell to a large complex cell through geologic time.

3.2. Life-cycle and -style of SPF lenticular microfossils

Lenticular microfossils comprise colonies, occasionally together with their composite structures, such as pairs and chains. Paired specimens corresponding to a sequence from fused to attached arrangements have also been identified both in petrographic thin sections and palynomorphic products (Fig. $5a_1$–a_4, b_1–b_3). Specimens and colonies suggestive of multiple fissions are present, but are very rare. Among the well-preserved colonies of the Goldsworthy locality ($n=230$) and the Panorama locality ($n=65$), fewer than 10 colonies appear to comprise a mixture of spheroids and lenses. Furthermore, clearly identified mixed colonies such as those that have been observed for younger (ca. 3.0 Ga) Farrel Quartzite lenticular microfossils, suggestive of multiple fissions or spore formation (Fig. 6), have not been seen (Sugitani *et al.*, 2009; Sugitani, 2012). Thus, lenticular microfossils mostly represent vegetative cells reproduced simply by binary fission (Sugitani *et al.*, 2015a) (Fig. 5c). The supposed simple reproduction style is critical to this study because this trait allows one to discuss morphological variations of lenticular microfossils exclusively in a taxonomic context. As for lifestyle of microorganisms represented by lenticular microfossils, Oehler *et al.* (2017) suggested that lenticular organisms had a planktonic habit for at least some stages in their life cycle based on their carbon isotopic values, occurrence, morphology, and no association with microbial mat faces.

Downloaded by 185.50.251.62 from www.liebertpub.com at 08/28/18. For personal use only.

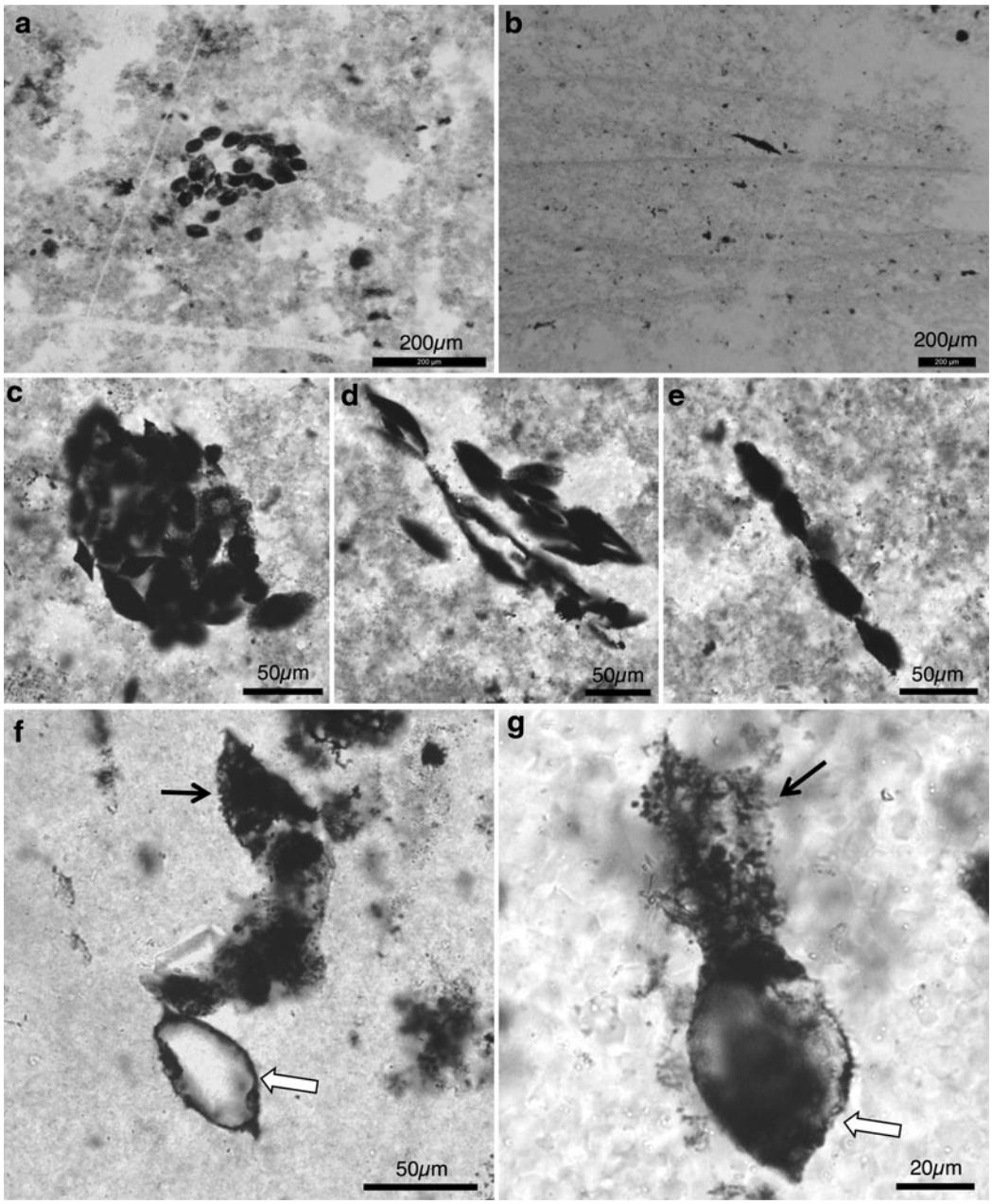

FIG. 4. **(a)** Colony of loosely clustered, carbonaceous lenticular microfossils embedded in the carbonaceous matrix of chert from the Panorama locality. **(b)** Cross-lamination identified by heterogeneous distribution of carbonaceous particles from the Goldsworthy locality. **(c)** Colony comprising tightly packed and randomly oriented individuals of lenticular microfossils from the Goldsworthy locality. **(d)** Colony comprising parallel oriented individuals of lenticular microfossils from the Goldsworthy locality. **(e)** Chain-like colony of lenticular microfossils from the Goldsworthy locality. **(f)** Lenticular microfossils showing different preservation status from the Panorama locality. The white arrow shows a well-preserved specimen with a continuous membrane-like wall, whereas the thin solid arrow shows a degraded specimen with a granular wall. **(g)** Paired lenticular microfossils showing heterogeneous degradation from the Waterfall locality. The white arrow shows a well-preserved counterpart, whereas the thin solid arrow shows a highly degraded one.

3.3. Trace element constraints on depositional environments

Post-Archean Australian shale (PAAS)-normalized patterns of (REE+Y) and abundance of heavy metals in analyzed microfossil-bearing black cherts are shown in Fig. 7.

PAAS-normalized patterns for fossil-bearing cherts from the Goldsworthy locality, except for three samples, vary from relatively flat to being enriched in light rare earth elements (LREEs) or middle rare earth elements (MREEs) (Table 1). A slight enrichment in heavy rare earth elements (HREEs; $Pr/Yb_{PAAS} = 0.69$) can be seen in only one sample (Fig. $7a_1$). The Eu anomaly ranges from 1.05 to 1.8. The Y/Ho ratios range

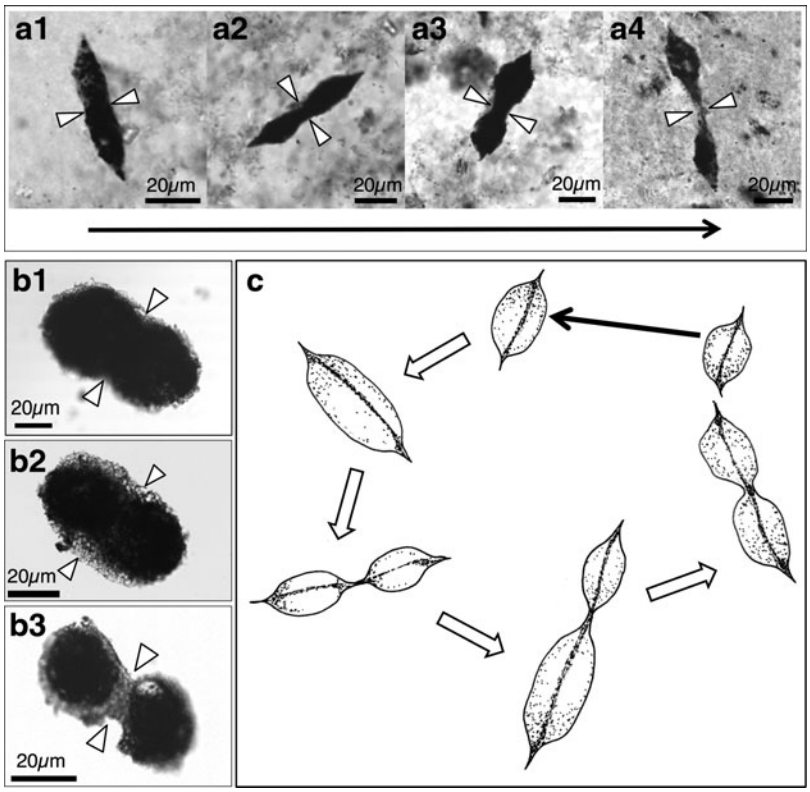

FIG. 5. Paired lenticular microfossils corresponding to a sequence of binary fissions; specimens in petrographic thin sections **(a_1–a_4)** and those in palynomorphs **(b_1–b_3)**. White triangular arrows show probable division plane. **(c)** Schematic figure showing a sequence of binary fissions of lenticular microfossils. White arrows show vegetative enlargement and subsequent division of lenticular cell. The thin solid arrow shows a complete liberation from chain-like colony.

Downloaded by 185.50.251.62 from www.liebertpub.com at 08/28/18. For personal use only.

from 27.1 to 35.4, similar to or slightly positively fractionated from chondritic values (26–27) (Pack *et al.*, 2007). All but one of the samples of chert are significantly enriched in Cr, Co, Ni, Cu, Zn, As, and Pb (Fig. $7a_2$). Total concentrations of these heavy metals range from 133 to 1276 ppm.

PAAS-normalized patterns for fossil-bearing cherts from the Panorama locality, as a whole, are distinct from those from the Goldsworthy locality (Fig. $7b_1$). Because of their low REE concentrations, their patterns are somewhat disordered. However, HREE and/or MREE enrichment relative

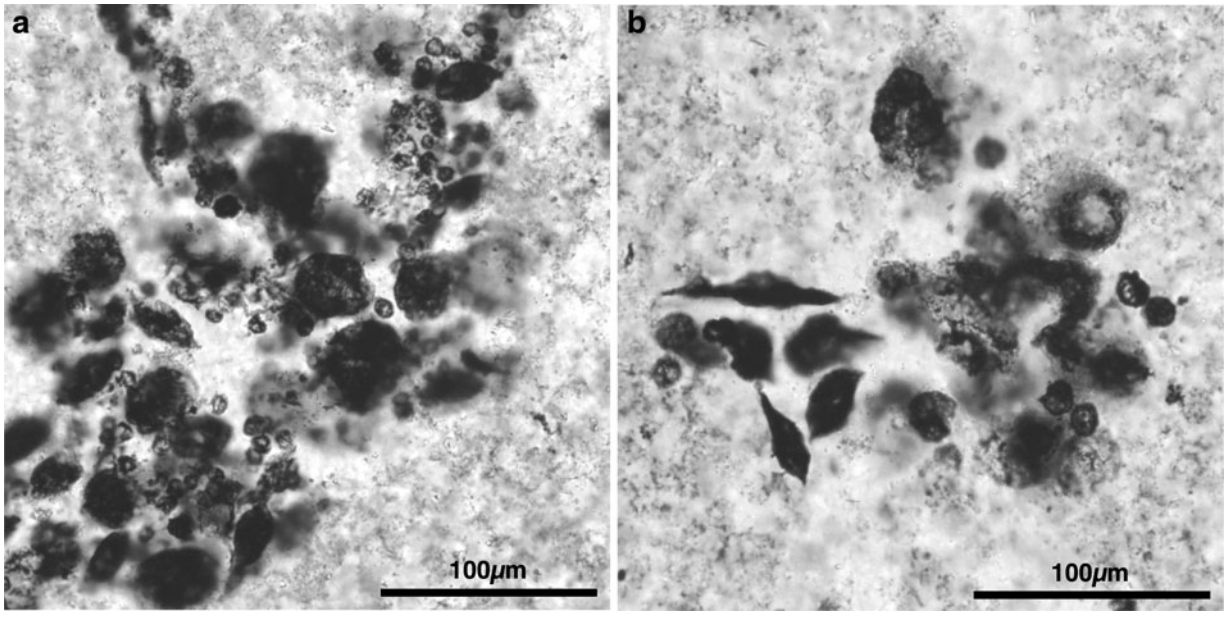

FIG. 6. Two examples of colonies of lenticular microfossils mixed with spheroid ones from the ca. 3.0 Ga Farrel Quartzite in the Pilbara Craton, Australia. Note the difference in density of individuals between colonies in **(a)** and **(b)** and that spheroids in **(a)** is significantly smaller than those in **(b)**, suggesting possible other aspect of diversity of lenticular microfossils.

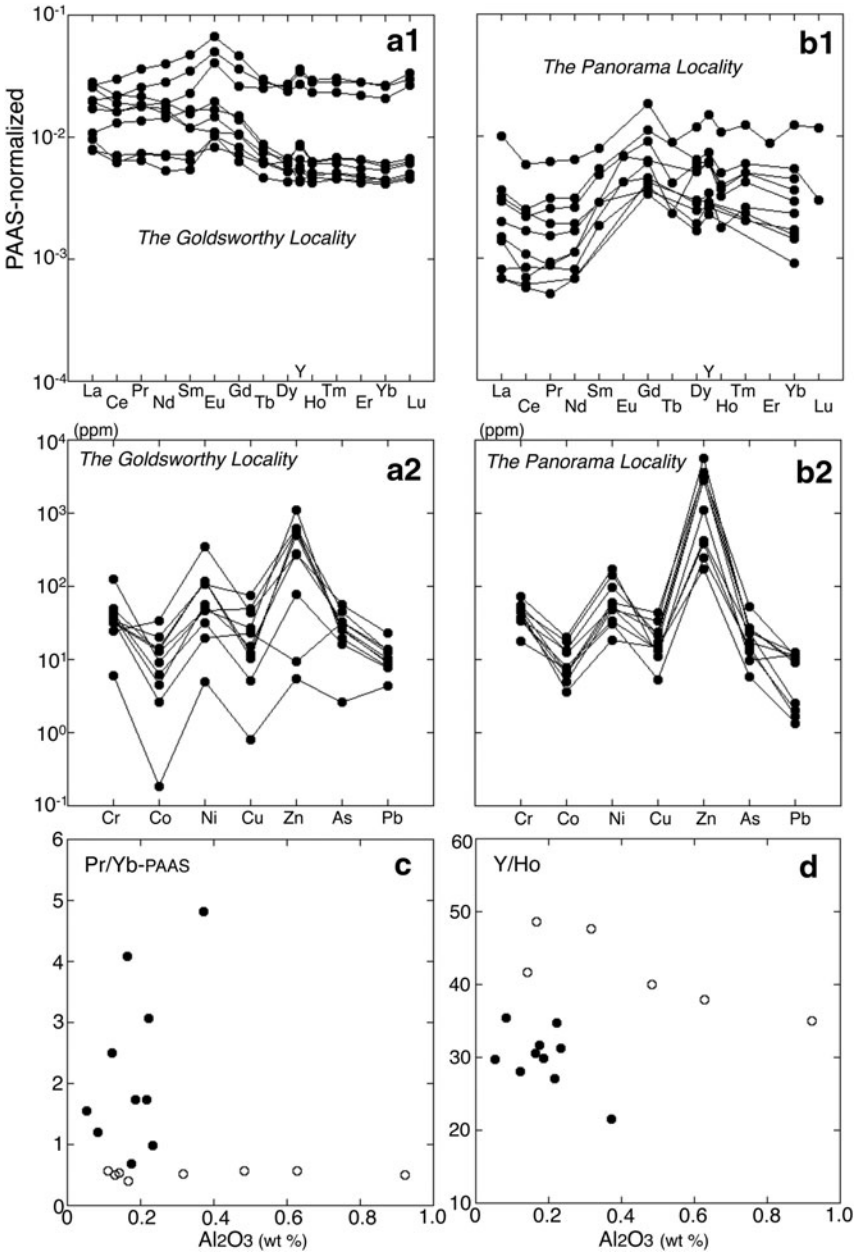

FIG. 7. PAAS-normalized REE + Y patterns and heavy metal abundance of fossil-bearing carbonaceous cherts from the Goldsworthy **(a_1, a_2)** and Panorama localities **(b_1, b_2)**. Data for the Goldsworthy samples are quoted from the study by Sugitani *et al.* (2015b). **(c, d)** Show relationships between Pr/Yb_{-PAAS} and Y/Ho with Al_2O_3 contents for fossil-bearing black cherts, respectively. Closed and open circles represent the Goldsworthy and Panorama samples, respectively. No correlations can be seen between Pr/Yb_{-PAAS} and Al_2O_3, and between Y/Ho and Al_2O_3, indicating that signatures of Pr/Yb_{-PAAS} and Y/Ho of the cherts are not affected by contaminated siliciclastic components. PAAS, post-Archean Australian shale; REE+Y = rare earth element (+ yttrium).

Downloaded by 185.50.251.62 from www.liebertpub.com at 08/28/18. For personal use only.

to LREE can be seen (Table 2). The Y/Ho ratios range from 35.1 to 48.6, significantly positively fractionated from chondritic values. All the analyzed black cherts are highly enriched in Cr, Co, Ni, Cu, Zn, As, and Pb (Fig. $7b_2$). Total concentrations of these heavy metals range from 259 to 5853 ppm. Their patterns are basically similar to those of the Goldsworthy samples, although enrichment of Zn is more pronounced.

Different REE+Y signatures between the Goldsworthy and Panorama chert samples described here cannot be explained by contamination by clastics (Fig. 7c, d), but can likely be attributed to differences in chemistry of the water masses from which the Goldsworthy and Panorama cherts precipitated. The results of trace element analyses are fully consistent with the fact that the two sedimentary successions, including the fossil-bearing cherts, display distinct lithostratigraphy (Fig. 2) and thus represent different depositional environments. According to previous studies, the depositional environment of the Goldsworthy fossil-bearing cherts was likely nonmarine and possibly equivalent to that of terrestrial hydrothermal system (Sugitani *et al.*, 2015b), whereas that of the Panorama fossil-bearing cherts is suggested to have been shallow marine (tidal zone), with inputs of hydrothermal fluids (Allwood *et al.*, 2007, 2010; Sugitani *et al.*, 2013).

3.4. Statistical analyses of the size distribution of lenticular microfossils

More than 1000 specimens of SPF microfossils were separated by acid maceration and prepared in slides, but 809 specimens ($n = 395$ and $n = 414$ for the Goldsworthy and Panorama populations, respectively) were selected for the following analyses by discarding fragmented specimens and outliers (see Section 2).

Table 1. Trace Element Data of Carbonaceous Black Cherts from the Goldsworthy Locality

	WF4	*WFL1-4A*	*WFL1-4B*	*WFL4-2*	*WF4SA*	*WF4SB*	*WF4SC*	*WF-mup1*	*WF-mup2*	*WF-mbo*
TiO_2 (wt %)	0.005	0.006	0.011	0.001	0.004	0.01	0.005	0.009	0.010	0.008
Al_2O_3	0.123	0.216	0.372	0.054	0.084	0.221	0.163	0.234	0.185	0.174
Fe_2O_3	0.159	0.047	0.122	0.236	0.441	0.331	0.383	0.424	0.497	1.12
Cr (ppm)	50.3	42.5	126	5.9	33.6	38.5	33.0	32.1	32.3	24.3
Co	13.1	6.2	9.2	0.18	20.2	4.5	2.6	13.4	14.4	33.9
Ni	48.1	32.0	46.9	4.9	106	55.5	19.5	117	119	349
Cu	27.2	5.1	50.3	0.81	74.7	15.0	23.1	10.2	12.2	44.0
Zn	1110	76.5	557	5.5	614	280	9.4	592	501	266
As	19.3	16.3	26.7	2.6	45.0	33.0	33.1	26.5	25.4	56.5
Pb	8.1	7.6	10.2	4.4	13.6	13.9	12.7	9.1	9.5	23.3
Σ Heavy metals	1276.1	186.2	826.7	24.3	907.1	440.3	133.4	800.3	713.8	797.0
La (ppm)	0.173	0.125	0.453	0.154	0.126	0.311	0.407	0.321	0.426	0.273
Ce	0.432	0.232	0.722	0.213	0.203	0.529	0.619	0.705	0.985	0.529
Pr	0.053	0.029	0.083	0.025	0.028	0.069	0.072	0.100	0.142	0.072
Nd	0.233	0.112	0.310	0.085	0.116	0.274	0.250	0.449	0.643	0.300
Sm	0.059	0.023	0.055	0.019	0.025	0.042	0.042	0.121	0.167	0.080
Eu	0.018	0.011	0.022	0.011	0.0091	0.012	0.016	0.055	0.073	0.045
Gd	0.049	0.021	0.046	0.027	0.024	0.035	0.035	0.120	0.153	0.086
Tb	0.0053	0.0028	0.0049	0.0037	0.0036	0.0045	0.0039	0.017	0.018	0.015
Dy	0.025	0.016	0.022	0.019	0.023	0.024	0.020	0.095	0.087	0.101
Y	0.132	0.090	0.085	0.107	0.174	0.169	0.115	0.687	0.538	0.729
Ho	0.0047	0.0033	0.0040	0.0036	0.005	0.0049	0.0038	0.022	0.018	0.023
Er	0.013	0.010	0.011	0.010	0.015	0.015	0.011	0.062	0.051	0.067
Tm	0.002	0.0014	0.0015	0.0014	0.0021	0.0020	0.0015	0.0090	0.0070	0.0090
Yb	0.012	0.0094	0.010	0.0091	0.013	0.013	0.010	0.057	0.046	0.059
Lu	0.002	0.0014	0.0015	0.0014	0.0020	0.0019	0.0015	0.009	0.008	0.010
Σ REEs	1.212	0.687	1.831	0.690	0.770	1.507	1.607	2.829	3.362	2.398
La/La* PAAS	0.93	0.94	1.09	1.01	1.07	1.03	1.0	0.94	0.89	0.95
Ce/Ce* PAAS	1.04	0.90	0.93	0.82	0.84	0.88	0.87	0.91	0.91	0.88
Eu/Eu* PAAS	1.19	1.76	1.49	1.80	1.21	1.05	1.46	1.54	1.59	1.74
Pr/Yb PAAS	2.49	1.73	4.82	1.55	1.20	3.06	4.09	0.99	1.74	0.69
Y/Ho	28.1	27.1	21.6	29.7	35.4	34.8	30.6	31.2	29.9	31.7

Data are quoted from our previous study (Sugitani *et al.*, 2015b).

Ce/Ce*PAAS = PAAS-normalized Ce anomaly = Ce/(Pr[Pr/Nd]); Eu/Eu*PAAS = PAAS-normalized Eu anomaly = Eu(0.67Sm + 0.33Tb); La/La*PAAS = PAAS-normalized La anomaly = La/(Pr[Pr/Nd]^2); PAAS = post-Archean Australian shale; REEs = rare earth elements.

Downloaded by 185.50.251.62 from www.liebertpub.com at 08/28/18. For personal use only.

Distribution patterns on the oblateness histogram (Fig. 8a, b) indicate that circular and oblate types dominate the Goldsworthy and Panorama populations, respectively. However, probability plots for oblateness are bent, suggesting that each population more likely comprises subpopulations (Fig. 8c). This was confirmed by cluster analyses using oblateness, area, and flange ratio as explanatory variables, indicating that each population is classified into three subpopulations (Fig. 9). The Goldsworthy population is dominated by two circular subpopulations of different areas ($n = 173$ and $n = 67$, respectively), with one slightly oblate subpopulation ($n = 155$). The Panorama population is also classified into three subpopulations, including two oblate types of different areas ($n = 222$ and $n = 65$, respectively) and one relatively circular type ($n = 127$). Results of multivariate analysis of variances show that these clusters are significantly different from each other in oblateness and/or area (Table 3). The same cluster analysis was performed for whole specimens, which comprise three circular subpopulations and two oblate subpopulations (Fig. 10). One of the circular subpopulations ($n = 242$) dominates the whole population and likely corresponds to integration of the Goldsworthy, slightly oblate, subpopulation ($n = 155$) and the Panorama, relatively circular, subpopulation ($n = 127$), certifying the validity of these cluster analyses.

3.5. Cause of morphological variations of SPF lenticular microfossils

3.5.1. Can cell growth and taphonomy explain morphological variations? Here, we consider causes of the observed variations in morphology (oblate and circular) of SPF lenticular microfossils in the context of cell growth and taphonomy. In general, cells grow vegetatively and enlarge their size before fission. As suggested from the reproduction model (Fig. 5), lenticular microbes likely elongated toward fission. Thus, the observed variation in oblateness could be attributed to cell elongation. However, there is no significant relationship between oblateness and the major dimension (Fig. 11). First, it is unrealistic to assume that only the Panorama population is dominated by individuals of a reproduction stage. In addition, neither taphonomy nor postdepositional deformation can explain the observed morphological variation. A partial loss of rim cannot be the cause of variation in oblateness because the central bodies of the two populations

TABLE 2. TRACE ELEMENT DATA OF CARBONACEOUS BLACK CHERTS FROM THE PANORAMA LOCALITY

	PAN-ipc1	*PAN-ipc2*	*PAN-ipc3*	*PAN-ipc4*	*PAN-ipc7*	*PAN-ipc8*	*PAN-ipc9*	*PAN-ipc10*	*PAN-ipc11*	*PAN-ipc12*
TiO_2 (wt %)	0.002	0.003	0.003	0.005	0.024	0.017	0.014	0.008	0.004	0.006
Al_2O_3	0.142	0.132	0.111	0.167	0.921	0.629	0.484	0.318	0.245	0.295
Fe_2O_3	0.005	0.054	0.025	0.059	0.372	0.145	0.166	0.302	0.437	0.645
Cr (ppm)	18.0	54.2	44.7	34.3	48.6	35.6	37.5	36.0	47.6	71.7
Co	7.43	12.6	3.63	7.82	6.65	5.01	6.14	13.2	17.9	20.1
Ni	30.8	51.8	18.2	34.3	59.7	47.5	53.2	95.8	141	170
Cu	5.30	13.2	14.6	13.9	43.7	33.7	23.7	21.8	17.4	10.9
Zn	247	418	171	378	3419	5695	3645	2768	2896	1090
As	14.8	22.9	5.74	12.9	53.1	23.8	27.2	27.2	17.5	9.82
Pb	1.65	2.55	1.34	2.05	11.0	12.6	9.79	9.19	11.5	11.7
Σ Heavy metals	325.0	575.3	259.2	483.3	3641.8	5853.2	3802.5	2971.2	3148.9	1384.2
La (ppm)	0.051	0.024	0.011	0.022	0.159	0.058	0.047	0.032	0.011	0.013
Ce	0.079	0.036	0.019	0.023	0.192	0.083	0.073	0.055	0.020	0.028
Pr	0.0075	0.0034	0.0020	0.0036	0.024	0.012	0.010	0.0059	ND	ND
Nd	0.031	0.018	0.011	0.018	0.103	0.050	0.042	0.027	0.011	0.013
Sm	0.010	0.010	ND	ND	0.028	0.019	0.017	0.010	ND	0.0065
Eu	0.0075	ND	ND	0.0046	ND	ND	0.0077	ND	ND	ND
Gd	0.021	0.012	0.011	0.015	0.061	0.037	0.030	0.020	0.014	0.013
Tb	ND	ND	ND	ND	0.0054	ND	0.0025	0.0014	ND	ND
Dy	0.019	0.0091	0.0062	0.0105	0.044	0.024	0.022	0.0200	0.011	0.0071
Y	0.121	0.052	0.046	0.068	0.298	0.148	0.124	0.119	0.058	0.056
Ho	0.0029	ND	ND	0.0014	0.0085	0.0039	0.0031	0.0025	ND	ND
Er	0.011	0.0045	ND	0.0058	0.027	0.013	0.0110	0.0092	0.0051	ND
Tm	ND	ND	ND	ND	0.0028	ND	ND	ND	ND	ND
Yb	0.0079	0.0038	0.0020	0.0051	0.027	0.012	0.0098	0.0065	0.0034	0.0032
Lu	ND	ND	ND	ND	0.0035	0.0009	ND	ND	ND	ND
Σ REEs	0.369	0.173	0.108	0.177	0.983	0.461	0.399	0.309	0.134	0.140
La/La* PAAS	1.68	2.87	2.41	2.21	1.77	1.22	1.20	1.64	NC	NC
Ce/Ce* PAAS	1.25	1.61	1.51	0.92	1.00	0.83	0.87	1.23	NC	NC
Eu/Eu* PAAS	NC	NC	NC	NC	NC	NC	1.51	NC	NC	NC
Pr/Yb PAAS	0.54	0.51	0.56	0.40	0.50	0.56	0.58	0.51	NC	NC
Y/Ho	41.7	NC	NC	48.6	35.1	37.9	40.0	47.6	NC	NC

See Table 1 for calculations of indices such as La/La* PAAS.
NC = not calculated; ND = not detected.

Downloaded by 185.50.251.62 from www.liebertpub.com at 08/28/18. For personal use only.

also have different degrees of oblateness (Fig. 12), consistent with degrees of oblateness of the whole bodies (Fig. 8). Finally, there was no evidence of significant deformation of the host cherts that could have potentially modified the original morphology of microfossils. Fossil-bearing carbonaceous cherts comprise microcrystalline quartz grains, which are not elongated, but are equant, without preferred orientation of extinction. It is likely that lenticular microbes were permineralized and/or encapsulated by silica before sediment compaction, similar to the younger (ca. 3.0 Ga) microfossil-bearing carbonaceous cherts from the Farrel Quartzite of the Pilbara Craton (Oehler *et al.*, 2009; Delarue *et al.*, 2017), and that recrystallization from amorphous silica to microquartz did not result in redistribution of the organic matter-comprising cells. This interpretation is supported by the fact that lenticular microfossils extracted by acid maceration retained their original morphologies.

3.5.2. Interpretation in the context of environmental adaptation and speciation. The 3.4-billion-year-old lenticular microbes can be classified into several subtypes defined by variations in oblateness and area from the equatorial view. As previously discussed, it is unlikely that the observed morphological variations can be attributed to cell growth and taphonomy. So, how can one explain such morphological variations of very early life? It is noteworthy that the two localities from which the lenticular microfossils of different morphological types were obtained represent different sedimentary environments. The Goldsworthy locality likely preserves a nonmarine hydrothermal setting, possibly equivalent to a modern geyser field, whereas the Panorama locality represents a shallow marine intertidal to subtidal setting, with some influence of hydrothermal activity. Thus, physicochemical aspects of the water masses such as concentrations of nutrients, salinity, pH, and Eh were potentially distinct between the two habitats. Additionally, hydrodynamic features were plausibly different as tidal action comparable with or stronger in scale than that of the modern ocean existed during the Archean (Lathe, 2004; Varga *et al.*, 2006; Eriksson and Simpson, 2012). Lenticular microbes at the Panorama location were therefore likely subjected to stronger hydrodynamic action than those at the Goldsworthy site. Although environmental factors critical to the shapes of lenticular microbes cannot be specified, it is reasonable to suggest that the observed morphological variations in SPF lenticular microfossils are the consequence of differences in environments of the two habitats.

Microorganisms, as well as macroorganisms, may change their morphology in response to environmental fluctuations without genetic mutation (Young, 2007; Niklas, 2009), as

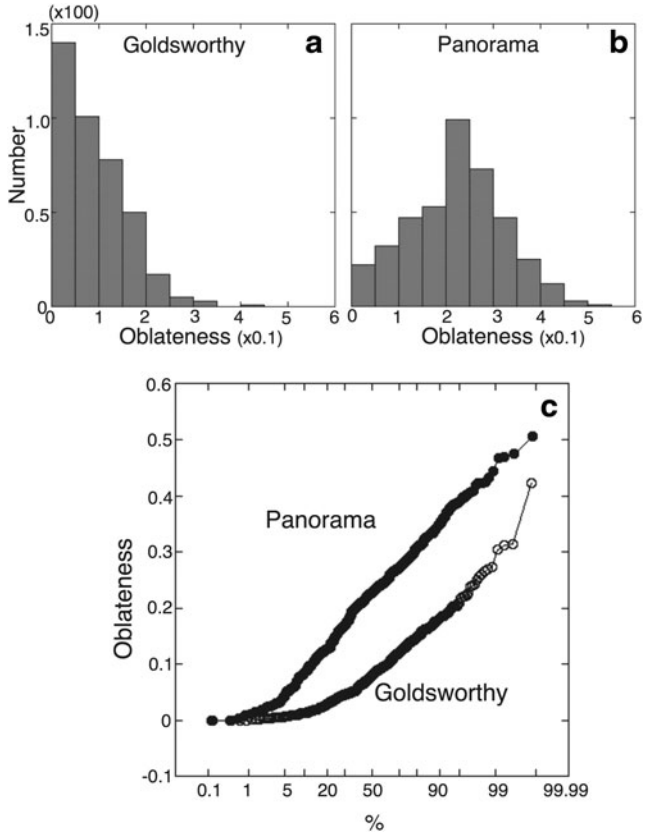

FIG. 8. **(a, b)** Histograms of oblateness for lenticular microfossils (whole bodies) from the Goldsworthy and Panorama localities. **(c)** Probability plots of oblateness. Note that patterns are not straight-lined, suggesting the presence of subpopulations with different degrees of oblateness.

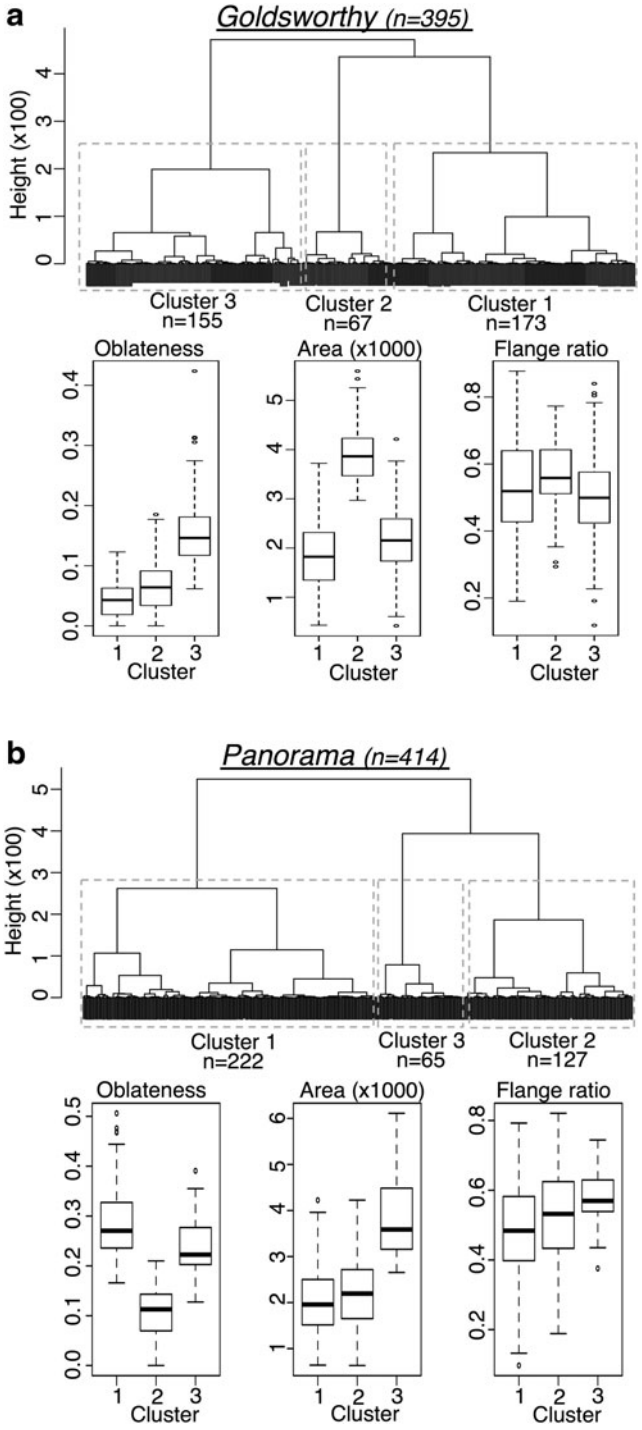

FIG. 9. Cluster dendrograms for the Goldsworthy population **(a)** and Panorama population **(b)** obtained by the Ward method, using oblateness, area, and area-based flange ratio as explanatory variables, and related box plots. Results of multiple tests obtained by using the Steel–Dwass method are given in Table 3.

exemplified by *Caulobacter crescentus*, which changes its stalk morphology depending on availability of nutrients such as phosphate (Brun and Janakiraman, 2000; Wagner *et al.*, 2006). Therefore, the described morphological variations of SPF microfossils can be explained as merely representing temporal and plastic alterations of cellular morphology. Alternatively, or more plausibly, variations could be the result of allopatric (geographic) and adaptive speciation for the following reasons. First, habitats of the two populations were spatially and environmentally isolated, providing conditions ideal for promoting speciation. Second, each population can be further classified into subpopulations, with a possible common type represented by cluster 3, obtained by cluster analyses of the whole specimens (Fig. 10). It seems unlikely that such hierarchical variations are the result of plastic alteration of cellular morphology as a means of temporal adaptation to environmental variations. Our suggestion that the SPF lenticular microfossils involve plural taxa is also consistent with the fact that lenticular microfossils comprise colonies of various occurrences (Fig. 4c–e), although correlation of colony type with the morphology of individual specimens cannot be made. Thus, results of this morphologic study provide examples and a model for speciation of Paleoarchean life and emphasize the significance of fossil records in studies of evolution (Benton and Pearson, 2001).

This study also suggests that the SPF lenticular microbes already had a highly organized cytoplasm, indispensable for such strict control of cell morphology. This is not unrealistic, even if lenticular microbes were prokaryotic, as it is now widely accepted that cytoskeletons long thought to be

Downloaded by 185.50.251.62 from www.liebertpub.com at 08/28/18. For personal use only.

TABLE 3. *T*- AND *P*-VALUES BETWEEN CLUSTERS

Oblateness	*Cluster 2*	*Cluster 3*	**Area**	*Cluster 2*	*Cluster 3*	**Flange ratio**	*Cluster 2*	*Cluster 3*
The Goldsworthy population								
Cluster 1	$t=3.4$, $p=0.018$	$t=15$, $p<0.0005$	*Cluster 1*	$t=11.8$, $p<0.0005$	$t=4$, $p<0.0005$	*Cluster 1*	$t=1.6$, $p=0.246$	$t=1.6$, $p=0.239$
Cluster 2		$t=9.5$, $p<0.0005$	*Cluster 2*		$t=11.3$, $p<0.0005$	*Cluster 2*		$t=3.4$, $p=0.0018$
The Panorama population								
Cluster 1	$t=15.5$, $p<0.0005$	$t=5.3$, $p<0.0005$	*Cluster 1*	$t=1.8$, $p=0.169$	$t=11.1$, $p<0.0005$	*Cluster 1*	$t=2.5$, $p=0.035$	$t=5.6$, $p<0.0005$
Cluster 2		$t=10.8$, $p<0.0005$	*Cluster 2*		$t=9.5$, $p<0.0005$	*Cluster 2*		$t=2.9$, $p=0.009$

specific to eukaryotes are common in archaea and bacteria (Ettema *et al.*, 2011; Shih and Rothfield, 2006; Wickstead and Gull, 2011; Celler *et al.*, 2013). Whatever their biological affinity, with a highly organized cytoskeleton, robust wall, and planktonic habit, Paleoarchean lenticular microbes, which were first reported from the Kaapvaal Craton in South Africa (possibly, Pflug, 1967; Walsh, 1992) and then from the Pilbara Craton in Western Australia (Sugitani *et al.*, 2010, 2013), were able to flourish and diversify on the early Earth and are believed to be one of the most successful organisms during this time (Oehler *et al.*, 2017).

Downloaded by 185.50.251.62 from www.liebertpub.com at 08/28/18. For personal use only.

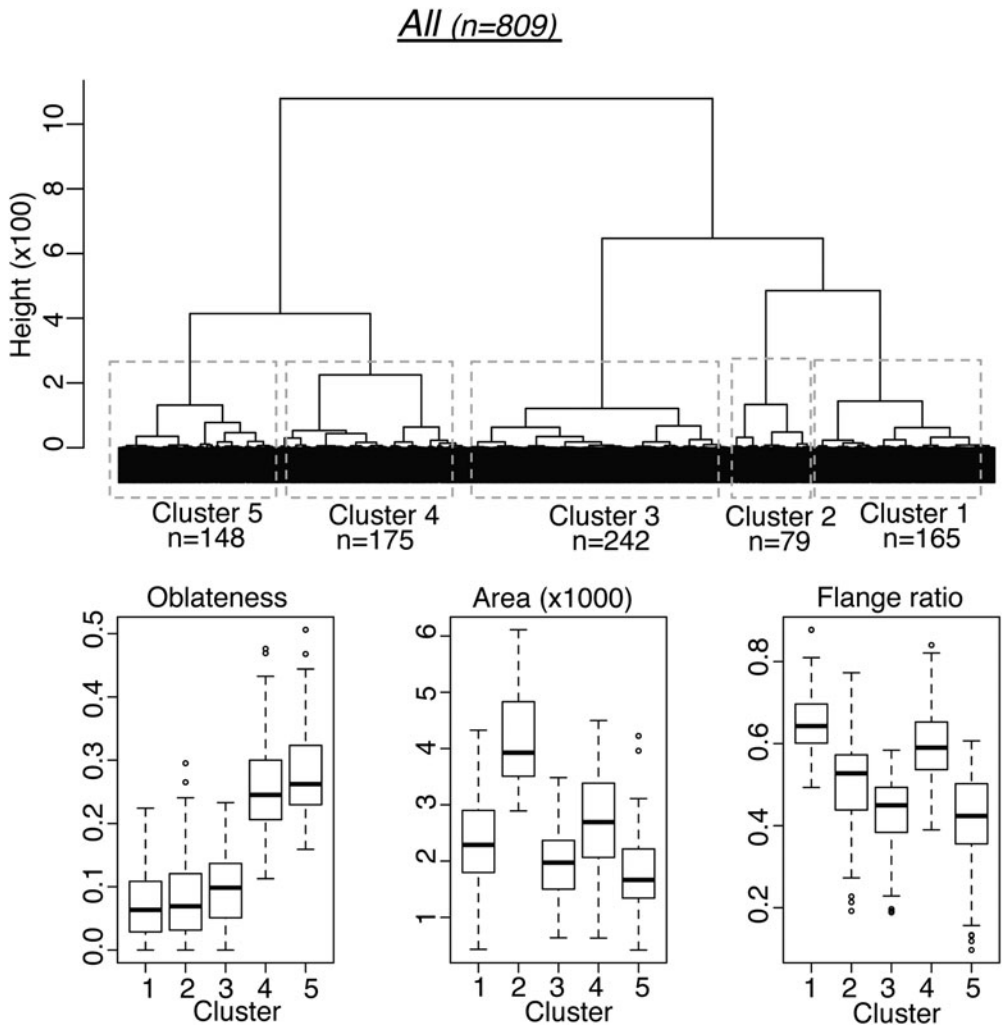

FIG. 10. Cluster dendrograms for the whole dataset obtained by the Ward method, using oblateness, area, and area-based flange ratio as explanatory variables, and related box plots.

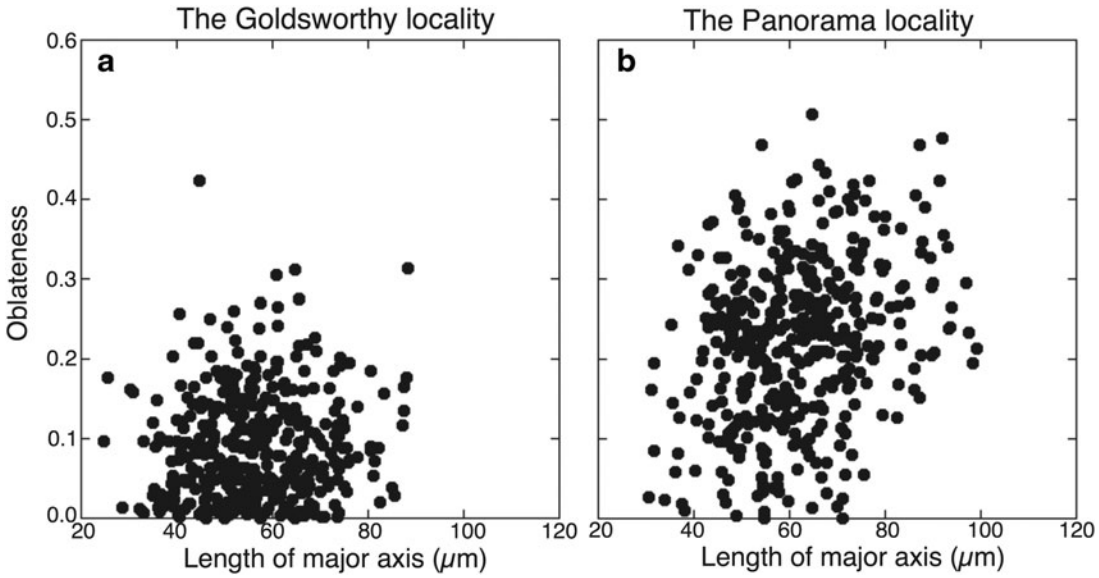

FIG. 11. Relationship between oblateness and the length of the major dimension of whole bodies for the Goldsworthy population **(a)** and Panorama population **(b)**.

Downloaded by 185.50.251.62 from www.liebertpub.com at 08/28/18. For personal use only.

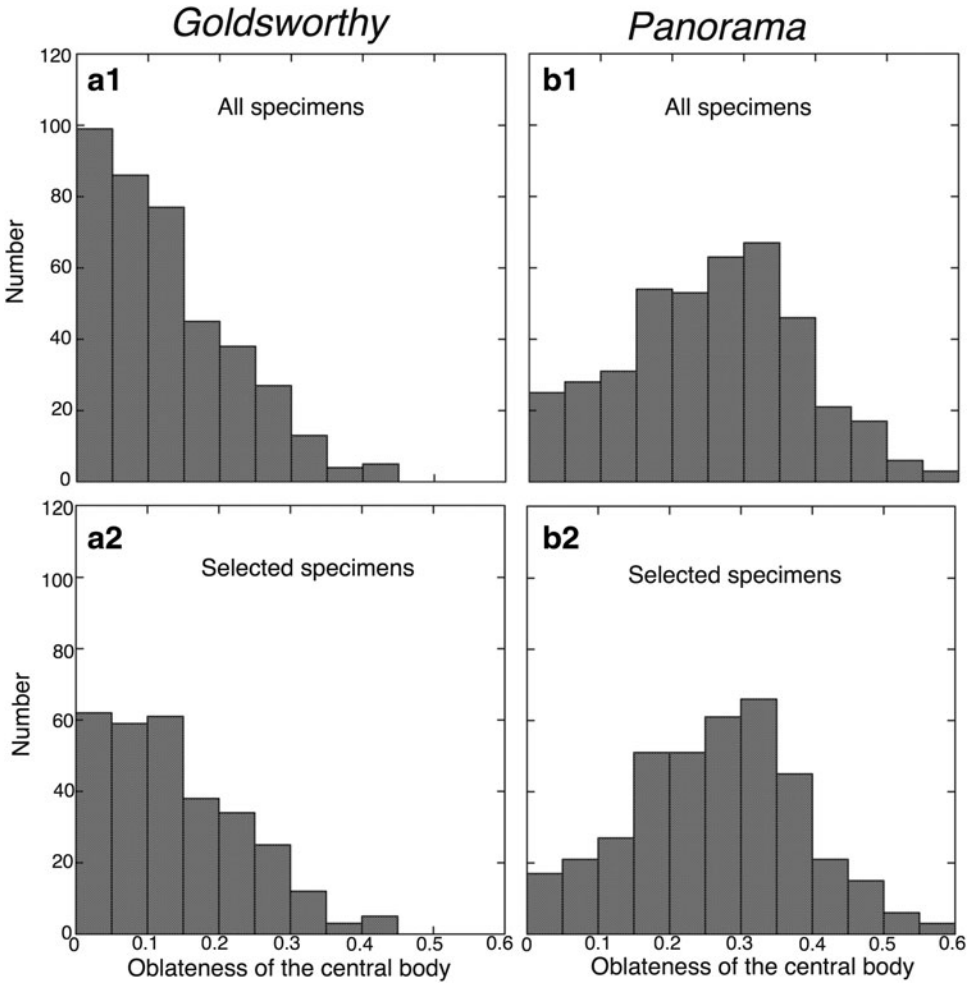

FIG. 12. Histograms for oblateness of central bodies of lenticular microfossils for the Goldsworthy population **(a)** and Panorama population **(b)**. All specimens **(a_1, b_1)** include specimens in which directions of major dimensions of their central bodies are inconsistent with those of whole bodies. Inconsistency is largely attributed to partial degradation of the central body. Selected specimens **(a_2, b_2)** correspond to those with directions of major dimensions of central bodies consistent with those of whole bodies.

4. Conclusions

Morphologies (area, oblateness, and flange ratio from an equatorial view) of lenticular microfossils from two localities ~80 km apart from the SPF (ca. 3.4 Ga) in the Goldsworthy and Panorama greenstone belts, Pilbara Craton of Australia, were statistically analyzed after extraction by acid maceration. The microfossil population ($n = 395$) from the Goldsworthy locality is dominated by a circular type, whereas the Panorama population ($n = 414$) by an oblate type. Cluster analyses further revealed that each population comprised three subpopulations defined by different areas and degrees of oblateness, one of which appears to be a common morphological type. Such variations in hierarchical structure cannot be explained by cell elongation toward fission, taphonomy, and deformation, but can be interpreted as original features of lenticular microbes. Lithostratigraphies of sedimentary successions at the two localities are distinct from one another, as are the trace element signatures, indicating that depositional environments of the host cherts and thus the habitats were different between the two localities. The described morphological variations are likely a direct consequence of allopatric (geographic) and adaptive speciation, although the possibility of temporal and plastic alterations of cellular morphology without genetic mutation cannot be ruled out entirely. In either case, lenticular microbes probably had a highly organized cytoskeleton indispensable for the strict control of morphology of such large and robust cells, providing advantages for their prosperity and diversification.

Downloaded by 185.50.251.62 from www.liebertpub.com at 08/28/18. For personal use only.

Acknowledgments

Financial support for K.S., K.M., and M.T. from the Japanese Society for the Promotion of Science (a grant-in-aid, Nos. 22340149 and 24654162) is gratefully acknowledged. Special thanks to Mariko Yamamoto and Natsuko Takagi, Nagoya University, for their assistance in XRF analyses of major elements of host cherts. K.S. also deeply acknowledges Dr. Martin J. Van Kranendonk and Dr. Kathleen Grey for their support in the field trip and Dr. Teruaki Nishikawa, Dr. Noelikanto Ramamonjisoa, Dr. Maud M. Walsh, and Dr. K. Yoda for critical and constructive comments on the preliminary manuscript.

Author Disclosure Statement

No competing financial interests exist.

References

Allwood, A.C., Walter, M.R., Kamber, B.S., Marshall, C.P., and Burch, I.W. (2006) Stromatolite reef from the Early Archaean era of Australia. *Nature* 441:714–718.

Allwood, A.C., Burch, I., and Walter, M.R. (2007) Stratigraphy and facies of the 3.43 Ga Strelley Pool Chert in the southwestern North Pole Dome, Pilbara Craton, Western Australia. *Geological Survey of Western Australia Record 2007/11*, Geological Survey of Western Australia, Perth.

Allwood, A.C., Kamber, B.S., Walter, M.R., Burch, I.W., and Kanik, I. (2010) Trace elements record depositional history of an Early Archean stromatolitic carbonate platform. *Chem Geol* 270:148–163.

Awramik, S.M., Schopf, J.W., and Walter, M.R. (1988) Carbonaceous filaments from North Pole, Western Australia: are they fossil bacteria in Archean stromatolites? A discussion. *Precam Res* 39:303–309.

Barghoorn, E.S. and Tyler, S.A. (1965) Microorganisms from the Gunflint Chert. *Science* 147:563–575.

Benton, M.J. and Pearson, P.N. (2001) Speciation in the fossil record. *Trends Ecol Evol* 16:405–411.

Brasier, M.D., Green, O.R., Jephcoat, A.P., Kleppe, A.K., Van Kranendonk, M.J., Lindsay, J.F., Steele, A., and Grassineau, N.V. (2002) Questioning the evidence for Earth's oldest fossils. *Nature* 416:76–81.

Brun, Y.V. and Janakiraman, R. (2000) The dimorphic life cycle of *Caulobacter* and stalked bacteria. In *Prokaryotic Development*, edited by Y.V. Brun and L.J. Shimkets, ASM Press, Washington, DC, pp 297–317.

Buick, R. (1984) Carbonaceous filaments from North Pole, Western Australia: are they fossil bacteria in Archaean stromatolites? *Precam Res* 24:157–172.

Celler, K., Koning, R.I., Koster, A.J., and van Wezel, G.P. (2013) Multidimensional view of the bacterial cytoskeleton. *J Bacteriol* 195:1627–1636.

Cloud, P.E., Jr. (1965) Significance of the Gunflint (Precambrian) microflora. *Science* 148:27–35.

Delarue, F., Robert, F., Sugitani, K., Tartèse, R., Duhamel, R., and Derenne, S. (2017) Investigation of the geochemical preservation of ca. 3.0 Ga permineralized and encapsulated microfossils by nanoscale secondary ion mass spectrometry. *Astrobiology* 17:1192–1202.

Engel, A.E.J., Nagy, B., Nagy, L.A., Engel, C.G., Kremp, G.O.W., and Drew, C.M. (1968) Alga-like forms in Onverwacht series, South Africa: oldest recognized lifelike forms on Earth. *Science* 161:1005–1008.

Eriksson, K.A. and Simpson, E. (2012) Precambrian tidal facies. In *Principles of Tidal Sedimentology*, edited by R.A. Davis, Jr. and R.W. Dalrymple, Springer, Berlin, pp 397–419.

Ettema, T.J.G, Lindås, A.-C., and Bernander, R. (2011) An actin-based cytoskeleton in arhcaea. *Mol Microbiol* 80:1052–1061.

Grey, K. and Sugitani, K. (2009) Palynology of Archean microfossils (c. 3.0 Ga) from the Mount Grant area, Pilbara Craton, Western Australia: further evidence for biogenicity. *Precam Res* 173:60–69.

Hickman, A.H. (2008) Regional review of the 3426-3350 Ma Strelley Pool Formation, Pilbara Craton, Western Australia. *Geological Survey of Western Australia, Record 2008/15*, Geological Survey of Western Australia, Perth.

Hickman, A.H. and Van Kranendonk, M.J. (2008) Archean crustal evolution and mineralization of the northern Pilbara Craton—a field guide. *Geological Survey of Western Australia, Record 2008/13*. Geological Survey of Western Australia, Perth.

Homann, M., Heubeck, C., Bontognali, T.R.R., Bouvier, A.-S., Baumgartner, L.P., and Airo, A. (2016) Evidence for cavity-dwelling microbial life in 3.22 Ga tidal deposits. *Geology* 44: 51–54.

Javaux, E.J., Marshall, C.P., and Bekker, A. (2010) Organic-walled microfossils in 3.2-billion-year-old shallow-marine siliciclastic deposits. *Nature* 463:934–938.

Knoll, A.H. (2014) Paleobiological perspectives on early eukaryotic evolution. *Cold Spring Harb Perspect Biol* 6:a016121.

Kremer, B. and Kaźmierczak, J. (2017) Cellularly preserved microbial fossils from ~3.4 Ga deposits of South Africa: a testimony of early appearance of oxygenic life? *Precam Res* 295:117–129.

Lathe, R. (2004) Fast tidal cycling and the origin of life. *Icarus* 168:18–22.

Lepot, K., Williford, K.H., Ushikubo, T., Sugitani, K., Mimura, K., Spicuzza, M.J., and Valley, J.W. (2013) Texture-specific

isotopic compositions in 3.4 Gyr old organic matter support selective preservation in cell-like structures. *Geochim Cosmochim Acta* 112:66–86.

Niklas, K.J. (2009) Functional adaptation and phenotypic plasticity at the cellular and whole plant level. *J Biosci* 34: 513–620.

Oehler, D.Z., Robert, F., Walter, M.R., Sugitani, K., Allwood, A., Meibom, A., Mostefaoui, S., Selo, M., Thomen, A., and Gibson, E.K. (2009) NanoSIMS: insights to biogenicity and syngeneity of Archaean carbonaceous structures. *Precam Res* 173:70–78.

Oehler, D.Z., Walsh, M.M., Sugitani, K., Liu, M.-C., and House, C.H. (2017) Large and robust, lenticular microorganismsm on the young Earth. *Precam Res* 296:112–119.

Pack, A., Russell, S.S., Shelley, J.M.G., and van Zuilen, M. (2007) Geo- and cosmochemistry of the twin elements yttrium and holmium. *Geochim Cosmochim Acta* 71:4592–4608.

Pflug, H.D. (1967) Structured organic remains from the Fig Tree Series (Precambrian) of the Barberton Mountain Land (South Africa). *Rev Palaeobot Palynol* 5:9–29.

Salman, V., Bailey, J.V., and Teske, A. (2013) Phylogenetic and morphologic complexity of giant sulphur bacteria. *Antonie van Leeuwenhoek* 104:169–186.

Schopf, J.W. (1976) Are the oldest ''fossils,'' fossils? *Orig Life Evol Biosph* 7:19–36.

Schopf, J.W. (1993) Microfossils of the Early Archean Apex Chert: new evidence of the antiquity of life. *Science* 260:640–646.

Schopf, J.W. and Walter, M.R. (1983) Archean microfossils: new evidence of ancient microbes. In *Earth's Earliest Biosphere, Its Origin and Evolution*, edited by J.W. Schopf, Princeton University Press, Princeton, NJ, pp 214–239.

Schopf, J.W., Kudryavtsev, A.B., Agresti, D.G., Wdowiak, T.J., and Czaja, A.D. (2002) Laser-Raman imagery of Earth's earliest fossils. *Nature* 416:73–76.

Schopf, J.W., Kudryavtsev, A.B., Osterhout, J.T., Williford, K.H., Kitajima, K., Valley, J.W., and Sugitani, K. (2017) An anaerobic ~3400 Ma shallow-water microbial consortium: presumptive evidence of Earth's Paleoarchean anoxic atmosphere. *Precam Res* 299:309–318.

Schopf, J.W., Kitajima, K., Spicuzza, M.J., Kudryavtsev, A.B., and Valley, J.W. (2018) SIMS analyses of the oldest known assemblage of microfossils document their taxon-correlated carbon isotope compositions. *Proc Natl Acad Sci U S A* 115:53–58.

Schulz, H.N. and Jørgensen, B.B. (2001) Big bacteria. *Annu Rev Microbiol* 55:105–137.

Shih, Y.-L. and Rothfield, L. (2006) The bacterial cytoskeleton. *Microbiol Mol Biol Rev* 70:729–754.

Sugitani, K. (2012) Life cycle and taxonomy of Archean flanged microfossils from the Pilbara Craton, Western Australia. In *34th International Geological Congress (IGC)*, Brisbane, 17.3, No. 257.

Sugitani, K., Grey, K., Nagaoka, T., Mimura, K., and Walter, M.R. (2009) Taxonomy and biogenicity of Archaean spheroidal microfossils (ca. 3.0 Ga) from the Mount Goldsworthy-Mount Grant area in the northeastern Pilbara Craton, Western Australia. *Precam Res* 173:50–59.

Sugitani, K., Lepot, K., Nagaoka, T., Mimura, K., Van Kranendonk, M., Oehler, D.Z., and Walter, M.R. (2010) Biogenicity of morphologically diverse carbonaceous microstructures from the ca. 3400 Ma Strelley Pool Formation, in the Pilbara Craton, Western Australia. *Astrobiology* 10:899–920.

Sugitani, K., Mimura, K., Nagaoka, T., Lepot, K., and Takeuchi, M. (2013) Microfossil assemblage from the 3400 Ma Strelley Pool Formation in the Pilbara Craton, Western Australia: results from a new locality. *Precam Res* 226:59–74.

Sugitani, K., Mimura, K., Takeuchi, M., Lepot, K., Ito, S., and Javaux, E.J. (2015a) Early evolution of large micro-organisms with cytological complexity revealed by microanalyses of 3.4 Ga organic-walled microfossils. *Geobiology* 13:507–521.

Sugitani, K., Mimura, K., Takeuchi, M., Yamaguchi, T., Suzuki, K., Senda, R., Asahara, Y., Wallis, S., and Van Kranendonk, M.J. (2015b) A Paleoarchean coastal hydrothermal field inhabited by diverse microbial communities: the Strelley Pool Formation, Pilbara Craton, Western Australia. *Geobiology* 13:522–545.

Van Kranendonk, M.J. (2007) A review of the evidence for putative Paleoarchean life in the Pilbara Craton, Western Australia. In *Earth's Oldest Rocks*, edited by M.J. Van Kranendonk, V. Bennett, and H. Smithies. Elsevier, Amsterdam, pp 855–877.

Varga, P., Rybicki, K.R., and Denis, C. (2006) Comment on the paper ''Fast tidal cycling and the origin of life'' by Richard Lathe. *Icarus* 180:274–276.

Wacey, D., Kilburn, M.R., Saunders, M., Cliff, J., and Brasier, M.D. (2011) Microfossils of sulphur-metabolizing cells in 3.4-billion-year-old rocks of Western Australia. *Nat Geosci* 4: 698–702.

Wagner, J.K., Setayeshgar, S., Sharon, L.A., Reilly, J.P., and Brun, Y.V. (2006) A nutrient uptake role for bacterial cell envelope extensions. *Proc Natl Acad Sci U S A* 103:11772–11777.

Walsh, M.M. (1992) Microfossils and possible microfossils from the Early Archean Onverwacht Group, Barberton Mountain Land, South Africa. *Precam Res* 54:271–293.

Walsh, M.M. and Lowe, D.R. (1985) Filamentous microfossils from the 3,500-Myr-old Onverwacht Group, Barberton Mountain Land, South Africa. *Nature* 314:530–532.

Waterbury, J.B. and Stanier, R.Y. (1978) Patterns of growth and development in pleurocapsalean cyanobacteria. *Microbiol Rev* 42:2–44.

Wickstead, B. and Gull, K. (2011) The evolution of the cytoskeleton. *J Cell Biol* 194:513–525.

Young, K.D. (2007) Bacterial morphology: why have different shapes? *Curr Opin Microbiol* 10:596–600.

Address correspondence to:
Kenichiro Sugitani
Department of Earth and Environmental Sciences
Graduate School of Environmental Studies
Nagoya University
Nagoya 464-8601
Japan

E-mail: sugi@info.human.nagoya-u.ac.jp

Submitted 28 November 2017
Accepted 27 January 2018

Abbreviations Used

HREE = heavy rare earth element
LREE = light rare earth element
MREE = middle rare earth element
PAAS = post-Archean Australian shale
REE = rare earth element
REE+Y = rare earth element (+ yttrium)
SPF = Strelley Pool Formation
XRF = X-ray fluorescence

Downloaded by 185.50.251.62 from www.liebertpub.com at 08/28/18. For personal use only.